Rate-Distortion-Optimization-Based Quantization Parameter Cascading Technique for Random-Access Configuration in H.265/HEVC

Yanchao Gong, Shuai Wan, *Member, IEEE*, Kaifang Yang, Yuan Yang, and Bo Li

***Abstract*— The random-access configuration is employed in H.265/HEVC video coding to make inter-frame prediction more efficient. The coding efficiency under the random-access configuration is closely related to the quantization parameter cascading (QPC) technique which determines the QP for encoding pictures in different temporal layers. The present QPC technique for the random-access configuration in H.265/HEVC is not optimized. In this paper, first, a rate-distortion-optimization-based technique for QPC, referred to as RDO-QPC, is proposed for the random-access configuration in H.265/HEVC. Based on the results from RDO-QPC, a simplified QPC technique, referred to as SRDO-QPC, is proposed. The experimental results verify the efficiency of the proposed two QPC techniques. Compared with the original configuration of QPC in H.265/HEVC, RDO-QPC achieves an average gain of 0.19 dB in ΔPSNR and an average reduction of 4.87% in ΔBR, while SRDO-QPC achieves an average gain of 0.17 dB in ΔPSNR and an average reduction of 4.32% in ΔBR. These two QPC techniques can both be used in practical situations, meeting different requirements of computational complexity.**

***Index Terms*— H.265/HEVC, quantization parameter cascading (QPC), random-access configuration, rate-distortion (R-D) optimization, video coding.**

I. Introduction

In H.264/AVC/SVC video coding [1], the hierarchical prediction structure [1]–[3] is proposed to achieve temporal scalability as well as to improve coding efficiency. In the latest High Efficiency Video Coding (H.265/HEVC) [4], [5], a similar hierarchical prediction structure is used, i.e., the random-access configuration, to achieve random access and to make inter-frame prediction more efficient for encoding [6]. When the random-access configuration is used, frames or pictures are organized into temporal layers, where pictures in different layers are of different importance in terms of prediction. The coding efficiency of the random-access configuration is determined by the quantization parameter (QP) selected for coding pictures in different temporal layers (i.e., the QP cascading (QPC) technique, referred to as QPC in this paper).

In H.264/AVC/SVC, the QPC technique proposed in JVT-P014 [3] for the hierarchical prediction structure has been widely adopted due to its good performance in terms of objective rate-distortion (R-D) performance. It is mentioned in [7] that although the QPC technique in [3] is effective, it is rather empirical and not adaptive. An adaptive QPC technique is theoretically derived in [7], where the R-D performance of QP cascaded hierarchical video coding is analyzed with a dependent R-D function. It is seen that [7] is most effective for video sequences with slow motion, and the widely accepted empirical QPC technique in [3] is actually an approximation to the theoretical solution in video sequences with fast motion.

Compared with H.264/AVC/SVC, new coding structures and techniques have been used in H.265/HEVC [4], [5], which make the QPC techniques in [3] and [7] not suitable for or unable to be directly applied to H.265/HEVC. Targeting at H.265/HEVC, a QPC technique is designed for the random-access configuration [6], which is generally considered as the default configuration or suggestion. The methods for QP selection in [8]–[10] can also be regarded as QPC techniques. However, those QPC techniques are not optimized in terms of R-D performance. How to select the QP for H.265/HEVC under the random-access configuration still remains open. This paper is devoted to R-D optimized QPC for the random-access configuration in H.265/HEVC based on theoretical analysis.

The rest of this paper is organized as follows. Section II briefly introduces the hierarchical prediction structure and the related QPC techniques in H.264/AVC/SVC and H.265/HEVC. Two R-D-optimization-based QPC techniques for the random-access configuration are proposed in Section III with their performance evaluation provided in Section IV. Conclusions are drawn in Section V.

II. Hierarchical Prediction Structure and Related QPC Techniques

A. Hierarchical Prediction Structure

In H.264/AVC/SVC, the hierarchical prediction structure contains two specific implementations [1]–[3], i.e., the hierarchical B structure as shown in Fig. 1 and the

Manuscript received May 28, 2015; revised September 14, 2015, November 19, 2015, and January 11, 2016; accepted February 28, 2016. Date of publication March 8, 2016; date of current version June 5, 2017. This work was supported by the National Natural Science Foundation Research Program of China under Grant 61371089 and Grant 61571337. This paper was recommended by Associate Editor A. Kaup.

The authors are with the School of Electronics and Information, Northwestern Polytechnical University, Xi'an 710072, China (e-mail: ycgong@mail.nwpu.edu.cn; swan@nwpu.edu.cn; kfyangnpu@mail.nwpu.edu.cn; yangnwpu@mail.nwpu.edu.cn; libo.npu@nwpu.edu.cn).

Color versions of one or more of the figures in this paper are available online at http://ieeexplore.ieee.org.

Digital Object Identifier 10.1109/TCSVT.2016.2539718

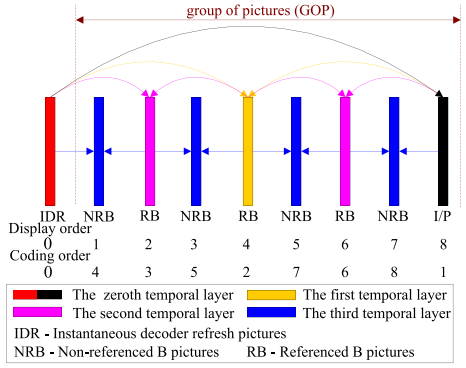

Fig. 1. Hierarchical B structure with four temporal layers and GOP = 8 in H.264/AVC/SVC.

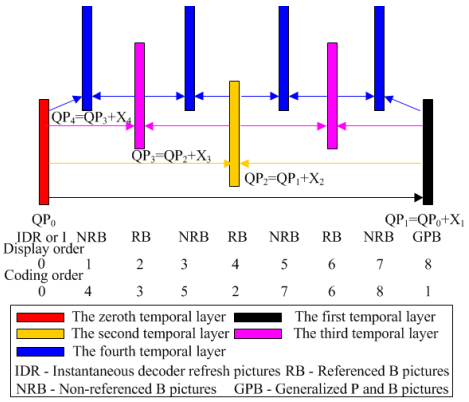

Fig. 2. Graphical presentation of random-access configuration in H.265/HEVC.

hierarchical P structure. In the latest H.265/HEVC, three kinds of prediction structures are used in the common test conditions [11], i.e., intra-only, low-delay, and random-access. For the random-access test condition, as shown in Fig. 2, a hierarchical B structure is used for encoding, where *I* frames are periodically inserted to realize random access.

By comparing Figs. 1 and 2, it is seen that the hierarchical B structure and random-access configuration are similar in the following ways. First, the first pictures in the video are all encoded as instantaneous decoder refresh (IDR) pictures. Second, the pictures that are bidirectionally predicted are encoded as referenced B pictures, and the B pictures in the highest temporal layers are nonreferenced B pictures. On the other hand, there are differences between these two structures as well. That is, they have different definitions in temporal layers regarding prediction. In the hierarchical B structure, I (including IDR) and P frames belong to the lowest temporal layer, i.e., the zeroth temporal layer. However, in the random-access configuration, all I (including IDR) frames are classified as the zeroth temporal layer, and the generalized P and B pictures belong to the first temporal layer.

For both the hierarchical B structure and the random-access configuration, generally speaking, pictures in a lower temporal layer are of more importance in prediction since they are directly or indirectly referenced by pictures in higher temporal layers. To improve the coding efficiency in terms of the overall R-D performance, a smaller QP is always preferred in a lower temporal layer and the QP is usually assigned in an increasing order with the increase of temporal layers. This is the general idea of a QPC technique [3], [6], [7], as formulated in

$$\mathrm{QP}_l = \mathrm{QP}_{l-1} + x_l, \quad l \geq 1 \tag{1}$$

where QP_0 is the QP for coding frames in the lowest temporal layer. How to select the QP offset, i.e., x_l, for each temporal layer is critical for improving the coding efficiency.

B. Related QPC Techniques

For the hierarchical B structure in H.264/AVC/SVC, the QPC technique in [3] is generally applied. Through analyzing the R-D performance of QP cascaded hierarchical video coding in H.264/AVC/SVC using the dependent R-D function, an adaptive QPC technique is implemented using lookup tables as an approximation to the optimal solution [7]. As the result, the optimal QP offset for the first temporal layer is approximately 4 for video sequences with fast motion, which is the same as [3], while [7] is most effective for video sequences with slow motion. It is seen that [3] is actually an approximation to the theoretically optimal solution in sequences with fast motion.

However, since new coding structures and techniques are introduced in H.265/HEVC compared with H.264/AVC/SVC, the application of [7] in H.265/HEVC is not straightforward. Furthermore, the spirit of [7] is based on Lagrangian optimization, where the optimal QP offset is obtained through finding out the derivation of the R-D function. However, the derivation is not actually taken since it is hard to find a closed solution. Alternatively, the optimal QP offset is obtained using lookup tables by exploiting typical values of certain parameters in the R-D function, where the typical values were empirically collected for H.264/AVC/SVC.

For the random-access configuration in H.265/HEVC, the QPC technique in [6] is generally considered as the default setting or suggestion. Apart from that, the adaptive QP rounding methods in [8] and [9], and the QP determination method using the lambda value in [10] can also be regarded as QPC techniques. However, those QPC techniques are all not optimized in terms of R-D performance. In the next section, based on the theoretical analysis and experimental observations, two R-D-optimization-based QPC techniques are proposed. In this paper, the R-D function is first established, then simplified using characteristics of H.265/HEVC, and finally theoretically derived to obtain the optimal QP offset.

III. Rate-Distortion-Optimization-Based QPC Techniques for Random-Access Configuration

The goal of this section is to find the optimal values of $x_l, l \geq 1$ in (1) to obtain higher objective R-D performance. Following the spirit of Lagrangian optimization, the total cost function is shown in:

$$J = \sum_{l=0}^{L-1} J_l = \sum_{l=0}^{L-1} (N_l(D_l + \lambda_l R_l)) \tag{2}$$

where, J_l, N_l, and λ_l stand for the cost, the number of frames, and the Lagrangian factor of the lth temporal

TABLE I
MAIN ENCODING PARAMETERS

codec	HM14.0 [12]
encoding structure	random-access configuration
profile	main
intra period	approximately one second [6][11]
GOP size	4, 8
QP_0	22, 27, 32, 37
search range	64
SAO	ON

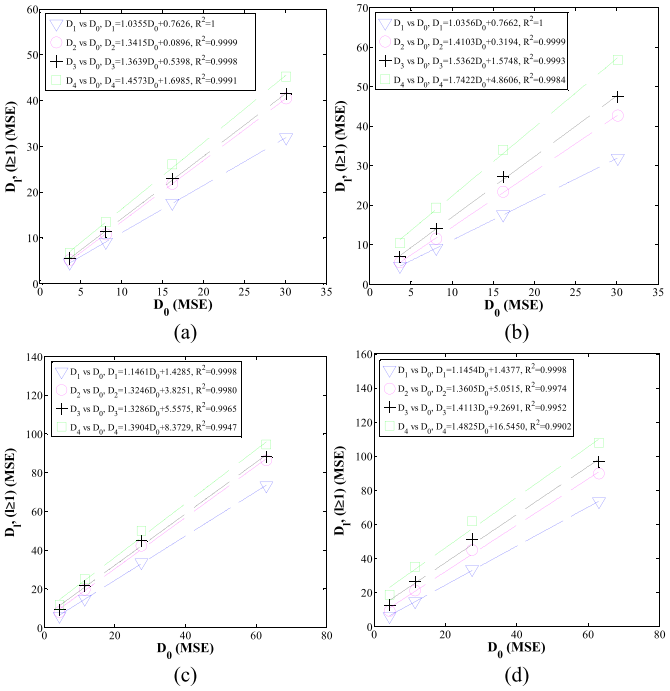

Fig. 3. $D_l, (l \geq 1)$ versus D_0 (GOP = 8). (a) *BasketballDrill* $x_1 = x_2 = x_3 = x_4 = 1$. (b) *BasketballDrill* $x_1 = 1, x_2 = 2, x_3 = 3, x_4 = 4$. (c) *PartyScene* $x_1 = x_2 = x_3 = x_4 = 1$. (d) *PartyScene* $x_1 = 1, x_2 = 2, x_3 = 3, x_4 = 4$.

layer, respectively. L means the total number of temporal layers. D_l and R_l represent the average distortion and bit-rate per frame of the lth temporal layer, respectively.

First, experiments were carried out to find out the relationship of the average distortion (measured by the mean-squared error of the luminance signal) and the bit-rate between higher temporal layers and the zeroth temporal layer. The main encoding parameters are listed in Table I, and the other parameters are set the same as indicated in the default configuration file of *encoder_randomaccess_main* [12].

As shown in Fig. 3, where the fitting function and fitting accuracy are also given in the legend, the experimental data verify that $D_l, l \geq 1$ and D_0 meet the linear relationship, that is

$$D_l = a_{l0} D_0 + b_{l0}. \tag{3}$$

The fitting accuracy is evaluated by the square of correlation coefficient (R^2) [13].

As shown in Fig. 4, it is observed that $R_l, l \geq 1$ and R_0 meet the power relationship, that is

$$R_l = c_{l0} R_0^{d_{l0}}. \tag{4}$$

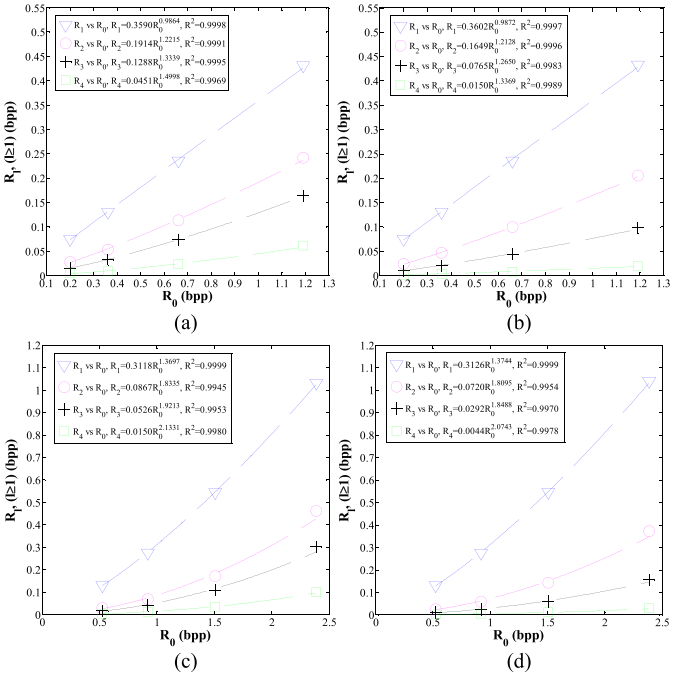

Fig. 4. $R_l, (l \geq 1)$ versus R_0 (GOP = 8). (a) *BasketballDrill* $x_1 = x_2 = x_3 = x_4 = 1$. (b) *BasketballDrill* $x_1 = 1, x_2 = 2, x_3 = 3, x_4 = 4$. (c) *PartyScene* $x_1 = x_2 = x_3 = x_4 = 1$. (d) *PartyScene* $x_1 = 1, x_2 = 2, x_3 = 3, x_4 = 4$.

In Figs. 3 and 4, two groups of experimental data are given as examples, with $x_1 = x_2 = x_3 = x_4 = 1$ and $x_1 = 1, x_2 = 2, x_3 = 3, x_4 = 4$. It should be noted that the relationships in (3) and (4) still hold when $x_l (x_l > 0, l \geq 1)$ changes. Substituting (3) and (4) into (2), we have

$$J = \left(N_0 + \sum_{l=1}^{L-1} (N_l a_{l0})\right) D_0 + \sum_{l=1}^{L-1} (N_l b_{l0}) + N_0 \lambda_0 R_0 + \sum_{l=1}^{L-1} \left(N_l \lambda_l c_{l0} R_0^{d_{l0}}\right). \tag{5}$$

In H.265/HEVC, the bit-rate and Lagrangian factor have the power relationship [13], that is

$$R = \gamma \lambda^{\sigma}. \tag{6}$$

And the distortion and bit-rate also meet the power relationship [13], that is

$$D = C R^K. \tag{7}$$

Equation (6) is substituted into (7) to get

$$D = C R^K = C \gamma^K \lambda^{\sigma K} = \alpha \lambda^{\beta}. \tag{8}$$

Then, the following can be obtained by substituting (6) and (8) into (5):

$$J = \left(N_0 + \sum_{l=1}^{L-1} (N_l a_{l0})\right) \alpha_0 \lambda_0^{\beta_0} + \sum_{l=1}^{L-1} (N_l b_{l0}) + N_0 \gamma_0 \lambda_0^{\sigma_0 + 1} + \sum_{l=1}^{L-1} \left(N_l c_{l0} \gamma_0^{d_{l0}} \lambda_0^{\sigma_0 d_{l0}} \lambda_l\right). \tag{9}$$

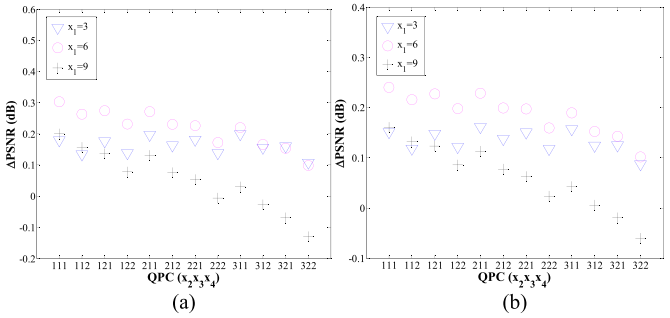

Fig. 5. Objective R-D performance of different QPC techniques (GOP = 8, $x_2 = 1, 2, 3$, $x_3 = 1, 2$, $x_4 = 1, 2$, QP_0 as shown in Table I). (a) *BasketballDrill*. (b) *PartyScene*.

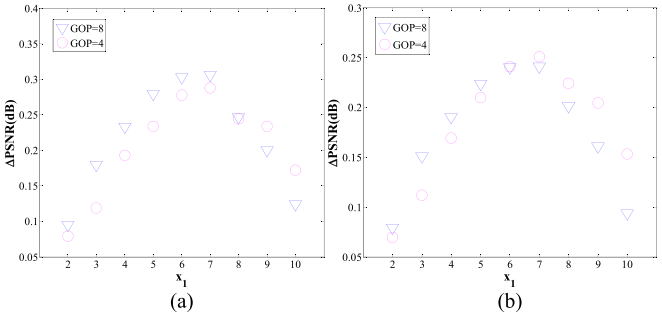

Fig. 6. GOP versus x_1 (GOP = 4, 8, $x_1 = 1, 2 \ldots 10$, and $x_l, l \geq 2 = 1$). (a) *BasketballDrill*. (b) *PartyScene*.

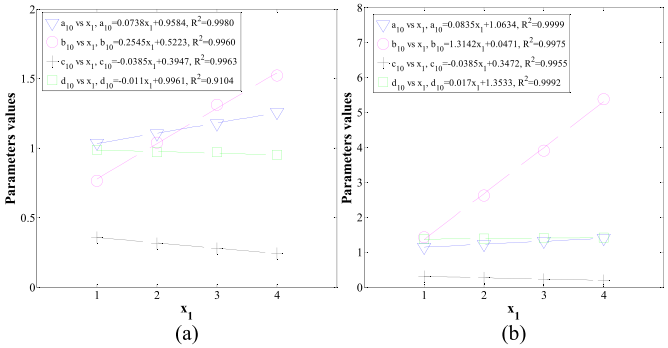

Fig. 7. x_1 versus a_{10}, b_{10}, c_{10}, d_{10} (GOP = 8, $x_1 = 1, 2, 3, 4$, and $x_2 = x_3 = x_4 = 1$). (a) *BasketballDrill*. (b) *PartyScene*.

It is seen that the QP and Lagrangian factor have the logarithm relationship [10], that is

$$\mathrm{QP} = a\ln(\lambda) + b \tag{10}$$

where a and b are 4.2005 and 13.7122, respectively. Combining (1) and (10), λ_l is represented as

$$\lambda_l = e^{\left(\frac{QP_0 + \sum_{i=1}^{l} x_i - b}{a}\right)}. \tag{11}$$

Then, the cost function is expressed as the following by substituting (11) into (9):

$$\begin{aligned} J = &\left(N_0 + \sum_{l=1}^{L-1}(N_l a_{l0})\right)\alpha_0 e^{\left(\frac{QP_0-b}{a}\right)\beta_0} + \sum_{l=1}^{L-1}(N_l b_{l0}) \\ &+ N_0\gamma_0 e^{\left(\frac{QP_0-b}{a}\right)(\sigma_0+1)} \\ &+ \sum_{l=1}^{L-1}\left(N_l c_{l0}\gamma_0^{d_{l0}} e^{\left(\frac{QP_0-b}{a}\right)\sigma_0 d_{l0}} e^{\left(\frac{QP_0+\sum_{i=1}^{l} x_i - b}{a}\right)}\right). \end{aligned} \tag{12}$$

In the following, three characteristics obtained from experimental observations are used to simplify (12).

Characteristic 1: As shown in Fig. 5, for various values of x_1, the QPC technique with $x_l, l > 1$ all set as 1 has the highest or near highest R-D performance in terms of ΔPSNR [14] with the QPC technique in [6] set as the benchmark. Here, different combinations of x_2, x_3, and x_4 are tested with $x_2 = 1, 2, 3$, $x_3 = 1, 2$, and $x_4 = 1, 2$. It should be noted that the same conclusion holds for the other QPC techniques which have larger values of $x_l, l > 1$.

Based on the above observation, it is the optimized value of x_1 in (1) that mostly determines the objective R-D performance, and $x_l, l > 1$ can be all set as 1. Accordingly, (12) is updated as

$$\begin{aligned} J = &\left(N_0 + \sum_{l=1}^{L-1}(N_l a_{l0})\right)\alpha_0 e^{\left(\frac{QP_0-b}{a}\right)\beta_0} + \sum_{l=1}^{L-1}(N_l b_{l0}) \\ &+ N_0\gamma_0 e^{\left(\frac{QP_0-b}{a}\right)(\sigma_0+1)} \\ &+ \sum_{l=1}^{L-1}\left(N_l c_{l0}\gamma_0^{d_{l0}} e^{\left(\frac{QP_0-b}{a}\right)\sigma_0 d_{l0}} e^{\left(\frac{QP_0+x_1+l-1-b}{a}\right)}\right). \end{aligned} \tag{13}$$

Characteristic 2: The optimal value of x_1 stays unchanged when GOP size is changing (where the QPC technique in [6] is also selected as the benchmark), as shown in Fig. 6. Since the number of temporal layers is actually determined by the GOP size, it is reasonable to find the optimized value of x_1 by considering a simplified case, where only two temporal layers are involved. And then, (13) is simplified as

$$\begin{aligned} J = &(N_0 + N_1 a_{10})\alpha_0 e^{\left(\frac{QP_0-b}{a}\right)\beta_0} + N_1 b_{10} + N_0\gamma_0 e^{\left(\frac{QP_0-b}{a}\right)(\sigma_0+1)} \\ &+ N_1 c_{10}\gamma_0^{d_{10}} e^{\left(\frac{QP_0-b}{a}\right)\sigma_0 d_{10}} e^{\left(\frac{QP_0+x_1-b}{a}\right)}. \end{aligned} \tag{14}$$

In (14), a_{10} and b_{10} are parameters representing the relationship between the average distortion per frame in the first temporal layer and that in the zeroth temporal layer. c_{10} and d_{10} are parameters representing the relationship between the average bit-rate per frame in the first temporal layer and that in the zeroth temporal layer. These four parameters are all related to x_1.

Characteristic 3: The relationships between a_{10}, b_{10}, c_{10}, d_{10}, and x_1 are all linear as shown in Fig. 7. Although, in Fig. 7, x_1 is selected as 1, 2, 3, and 4, it should be noted that the linear relationships between a_{10}, b_{10}, c_{10}, d_{10}, and x_1 still hold when x_1 has larger values. In our experiments, the largest x_1 has been set to 10 and the same conclusions can be drawn.

The values of a_{10}, b_{10}, c_{10}, and d_{10} in Fig. 7 have been determined using the least-squares method. That is, after encoding the video sequence using different QP_0 (i.e., 22, 27, 32 and 37 in Table I) and $x_l, l = 1, 2, 3, 4$, the corresponding D_0, D_1, R_0, and R_1 were collected. As shown in Fig. 8, the relationship between D_1 and D_0 is fitted using the

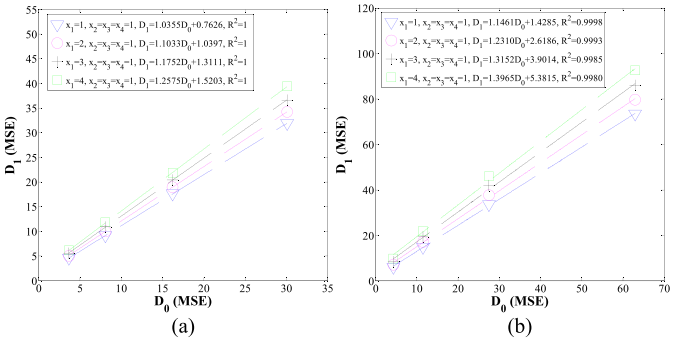

Fig. 8. D_1 versus D_0 (GOP = 8). (a) *BasketballDrill*. (b) *PartyScene*.

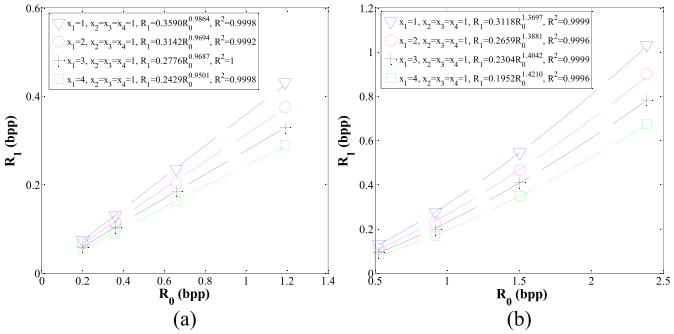

Fig. 9. R_1 versus R_0 (GOP = 8). (a) *BasketballDrill*. (b) *PartyScene*.

least-squares method to obtain a_{10} and b_{10}. Similarly, c_{10} and d_{10} can be determined by R_1 and R_0, as shown in Fig. 9.

Based on the third characteristic, we have

$$a_{10} = \mu_a x_1 + \eta_a, \quad b_{10} = \mu_b x_1 + \eta_b$$
$$c_{10} = \mu_c x_1 + \eta_c, \quad d_{10} = \mu_d x_1 + \eta_d. \tag{15}$$

Substituting (15) into (14) leads to (16), as shown at the bottom of this page, where μ_a, η_a, μ_b, η_b, μ_c, η_c, μ_d, and η_d are only related to the characteristics of video sequences. Here, a and b in (16) are constants [10]. α_0, β_0, γ_0, and σ_0 are the parameters in the zeroth temporal layer. So all model parameters in (16) are independent with x_1.

Set the derivation of J, i.e., $\partial J/\partial x_1$, to zero. Let $f(x) = \partial J/\partial x_1$, and the approximate solution of $\partial J/\partial x_1 = 0$ is $x_1 = \theta - f(\theta)/f(\theta)'$ [i.e., (17), as shown at the bottom of this page] using the Newton–Raphson method [15], where θ is empirically set as 6. The proposed RDO-QPC technique can be implemented as follows.

1) For a given video sequence, pre-encode the first two frames for six times with the settings of $\mathrm{QP}_0 = 22, 27, 37$, $x_1 = 1, 4$, and $x_l = 1, l > 1$, respectively.
2) After pre-encoding, D_1, D_0, R_1, R_0, and λ_0 are obtained. Then, the least-squares method is used for fitting the data. α_0 and β_0 can be obtained using (8), given D_0 and λ_0, and γ_0 and σ_0 can be found out using (6), given R_0 and λ_0.The values of a_{10}, b_{10}, c_{10}, and d_{10} are determined using D_1, D_0, R_1, and R_0, as described above, using data from pre-encoding, and then μ_a, η_a, μ_b, η_b, μ_c, η_c, μ_d, and η_d are achieved through fitting using (15). As the result, x_1 is obtained according to (17).
3) Finally $\mathrm{QP}_l, l \geq 1$ are set as follows:

$$\mathrm{QP}_l = \begin{cases} \mathrm{QP}_{l-1} + \lceil x_1 \rceil, & l = 1 \\ \mathrm{QP}_{l-1} + 1, & l > 1. \end{cases} \tag{18}$$

It should be noted that, in pre-encoding, $x_1 = 1, 4$ are used to collect data to model (3), (4), (6), (8), and (15) for simplicity and effectiveness. Applying more and larger values of x_1 has no influence to the model forms and the result of RDO-QPC.

Based on the results from RDO-QPC, a simpler QPC technique with a fixed value of x_1 (denoted as SRDO-QPC for short) is proposed. It is found that the average value of x_1 for all tested video sequences using RDO-QPC is around 5 (rounding up). Accordingly, SRDO-QPC sets $\mathrm{QP}_l, l \geq 1$ according to (1) with $x_1 = 5$ and $x_l (l > 1) = 1$. Compared with RDO-QPC, SRDO-QPC avoids pre-encoding at the cost of decrease in R-D performance. The performance of the two proposed QPC techniques is evaluated in the following section.

IV. Experimental Results and Discussions

In this paper, the QPC technique in [6] was used as the benchmark, and then the proposed RDO-QPC and SRDO-QPC were compared with [10]. $\mathrm{PSNR_{YUV}}$ as described in [16] has been used in performance evaluation, where the luminance and chroma signals are all considered. Given the bit-rate and $\mathrm{PSNR_{YUV}}$ values, ΔBR has been calculated using the piecewise cubic interpolation [11]. And ΔPSNR has been calculated using the excel macro provided in [14].

$$\begin{aligned} J = {} & (N_0 + N_1(\mu_a x_1 + \eta_a))\alpha_0 e^{\left(\frac{\mathrm{QP}_0 - b}{a}\right)\beta_0} + N_1(\mu_b x_1 + \eta_b) + N_0\gamma_0 e^{\left(\frac{\mathrm{QP}_0 - b}{a}\right)(\sigma_0+1)} \\ & + N_1(\mu_c x_1 + \eta_c)\gamma_0^{(\mu_d x_1 + \eta_d)} e^{\left(\frac{\mathrm{QP}_0 - b}{a}\right)\sigma_0(\mu_d x_1 + \eta_d)} e^{\left(\frac{\mathrm{QP}_0 + x_1 - b}{a}\right)} \end{aligned} \tag{16}$$

$$\begin{aligned} x_1 = \theta - \frac{ \begin{array}{l} \frac{\mu_a \alpha_0 e^{\left(\frac{\mathrm{QP}_0 - b}{a}\right)\beta_0} + \mu_b}{\gamma_0^{\mu_d\theta + \eta_d} e^{\frac{(\sigma_0\mu_d\mathrm{QP}_0 - \sigma_0\mu_d b + 1)\theta + \sigma_0\eta_d\mathrm{QP}_0 - \sigma_0\eta_d b + \mathrm{QP}_0 - b}{a}}} + \mu_c\left(1 + \theta\mu_d\ln(\gamma_0) + \frac{\theta(\sigma_0\mu_d\mathrm{QP}_0 - \sigma_0\mu_d b + 1)}{a}\right) \\ + \eta_c\left(\mu_d\ln(\gamma_0) + \frac{(\sigma_0\mu_d\mathrm{QP}_0 - \sigma_0\mu_d b + 1)}{a}\right) \end{array} }{ \begin{array}{l} \mu_c\left(2\mu_d\ln(\gamma_0) + \frac{2(\sigma_0\mu_d\mathrm{QP}_0 - \sigma_0\mu_d b + 1)}{a} + \theta\mu_d^2(\ln(\gamma_0))^2 + \frac{2\theta\mu_d\ln(\gamma_0)(\sigma_0\mu_d\mathrm{QP}_0 - \sigma_0\mu_d b + 1)}{a} + \theta\left(\frac{(\sigma_0\mu_d\mathrm{QP}_0 - \sigma_0\mu_d b + 1)}{a}\right)^2\right) \\ + \eta_c\left(\mu_d^2(\ln(\gamma_0))^2 + \frac{2\mu_d\ln(\gamma_0)(\sigma_0\mu_d\mathrm{QP}_0 - \sigma_0\mu_d b + 1)}{a} + \left(\frac{(\sigma_0\mu_d\mathrm{QP}_0 - \sigma_0\mu_d b + 1)}{a}\right)^2\right) \end{array} } \end{aligned} \tag{17}$$

TABLE II
VALUES OF x_1 SELECTED BY RDO-QPC TECHNIQUE

Class	Sequence name	Encoded frames	x_1 ($QP_0 = 22,27,32,37$)
A	Traffic	150	(4, 4, 4, 4)
	PeopleOnStreet	150	(3, 3, 4, 4)
	Nebuta	300	(4, 4, 4, 5)
	SteamLocomotive	300	(2, 2, 2, 2)
B	Kimono	240	(2, 2, 3, 3)
	ParkScene	240	(4, 4, 4, 4)
	Cacuts	500	(5, 5, 6, 6)
	BasketballDrive	500	(3, 3, 3, 3)
	BQTerrace	600	(3, 3, 3, 3)
C	BasketballDrill	500	(7, 7, 7, 7)
	BQMall	600	(5, 5, 5, 5)
	PartyScene	500	(7, 6, 6, 7)
	RaceHorses	300	(2, 2, 2, 2)
D	BasketballPass	500	(5, 5, 5, 5)
	BQSquare	600	(5, 5, 5, 5)
	BlowingBubbles	500	(7, 6, 6, 6)
	RaceHorses	300	(2, 2, 3, 3)
E	FourPeople	600	(6, 6, 6, 6)
	Johnny	600	(5, 5, 5, 5)
	KristenAndSara	600	(6, 6, 6, 6)
	Vidyo1	600	(6, 6, 6, 6)
	Vidyo3	600	(6, 6, 6, 6)
	Vidyo4	600	(6, 6, 6, 6)
F	BasketballDrillText	500	(7, 7, 7, 7)
	ChinaSpeed	250	(4, 4, 4, 4)
	SlideEditing	300	(2, 2, 2, 2)
	SlideShow	500	(4, 4, 4, 4)

TABLE III
OBJECTIVE R-D PERFORMANCE

Sequence name		[10]		RDO-QPC		SRDO-QPC	
		$\Delta PSNR$ (dB)	ΔBR (%)	$\Delta PSNR$ (dB)	ΔBR (%)	$\Delta PSNR$ (dB)	ΔBR (%)
Traffic		0.08	-2.68	0.13	-3.96	0.13	-3.96
PeopleOnStreet		0.08	-1.98	0.04	-0.93	0.03	-0.48
Nebuta		0.08	-3.70	0.04	1.14	0.03	2.31
SteamLocomotive		0.00	-0.35	0.00	0.74	-0.04	3.28
Kimono		0.04	-1.43	0.02	-0.89	0.01	-0.06
ParkScene		0.06	-2.14	0.08	-2.57	0.06	-2.04
Cacuts		0.06	-2.81	0.07	-2.53	0.07	-2.61
BasketballDrive		0.03	-1.33	0.01	-0.12	-0.04	1.96
BQTerrace		0.03	-2.16	0.06	-4.17	0.07	-5.58
BasketballDrill		0.13	-3.30	0.34	-8.53	0.31	-7.75
BQMall		0.08	-2.13	0.15	-4.04	0.15	-4.04
PartyScene		0.13	-3.42	0.32	-8.71	0.29	-7.65
RaceHorses		0.04	-1.25	0.00	0.10	-0.06	1.98
BasketballPass		0.09	-2.11	0.09	-2.05	0.09	-2.05
BQSquare		0.08	-2.33	0.25	-7.53	0.25	-7.53
BlowingBubbles		0.11	-2.95	0.24	-6.25	0.22	-5.74
RaceHorses		0.07	-1.66	0.01	-0.22	-0.02	0.60
FourPeople		0.12	-3.74	0.48	-11.82	0.42	-10.67
Johnny		0.08	-3.64	0.26	-8.73	0.26	-8.73
KristenAndSara		0.11	-3.90	0.36	-10.43	0.33	-9.77
Vidyo1		0.08	-2.83	0.34	-9.61	0.31	-8.87
Vidyo3		0.07	-2.71	0.39	-10.69	0.35	-9.72
Vidyo4		0.10	-3.73	0.38	-11.23	0.34	-10.44
BasketballDrillText		0.14	-3.27	0.35	-8.26	0.32	-7.46
ChinaSpeed		0.20	-4.29	0.26	-5.82	0.30	-6.77
SlideEditing		0.01	-0.08	0.00	0.02	-0.07	0.51
SlideShow		0.15	-1.88	0.35	-4.40	0.43	-5.40
Ave.	Classes A-D and F	0.08	-2.25	0.13	-3.29	0.12	-2.78
	All	0.08	-2.51	0.19	-4.87	0.17	-4.32

The tested video sequence database was established with 27 video sequences including all recommended sequences for the test of random-access configuration, as shown in Table II. The video sequences were encoded with the GOP size set to 8 and using encoding parameters as shown in Table I and in the configuration file *encoder_randomaccess_main* for HM.

A. QP Selection Results

In this section, the values of QPs that are selected by four QPC techniques for encoding pictures in different temporal layers are discussed. The QPs are easily found out by (1) if $x_l, l \geq 1$ are known. For the QPC technique in [6], RDO-QPC, and SRDO-QPC, the selected $x_l, l > 1$ are all 1, whereas the selected x_1 are different for these three QPC techniques. For the QPC technique in [6], RDO-QPC, and SRDO-QPC, the selected x_1 are 1, adaptive, and 5, respectively. Taking *PeopleOnStreet* as the example, the RDO-QPC chooses the values of x_1 as 3, 3, 4, and 4 for $QP_0 = 22$, 27, 32, and 37, respectively, as shown in Table II. And the values of $x_l, l \geq 1$ are determined by λ_l for the QPC technique in [10].

B. Objective R-D Performance and Complexity

Table III gives the objective R-D performance of different QPC techniques, where [6] is set as the benchmark. And the average ΔBR values are -4.87%, -4.32%, and -2.51% for RDO-QPC, SRDO-QPC, and [10], respectively, with all 27 video sequences used. Using the tested videos in Classes A–D and F only, the average ΔBR values are -3.29%, -2.78%, and -2.25% for RDO-QPC, SRDO-QPC, and [10], respectively. From this observation, we can conclude that the proposed methods are more effective to the head-and-shoulder video sequences (i.e., Classes E). However, the proposed RDO-QPC and SRDO-QPC always outperform the QPC techniques in [6] and [10] when various kinds of video sequences are considered. Therefore, although [6] has been recognized as the QPC technique recommended for H.265/HEVC, a larger x_1 should be chosen, especially for sequences with slow motion, such as Classes E. It is noted that for the sequences with fast motion, such as *RaceHorses*, the performance of the proposed RDO-QPC is limited. This is because that for such sequences, video content between the first two frames and the following is likely to be quite different, which makes the parameters estimation not accurate enough and leads to the slight loss in the performance of the proposed RDO-QPC.

The R-D curves for *BasketballDrill* sequence are shown in Fig. 10 as examples. Fig. 10(a) shows R-D curves at the same QP_0, i.e., 22, 27, 32, and 37. And Fig. 10(b) shows the R-D curves at similar bit-rates, where the QP_0 was set differently for four compared QPC techniques since different x_l are chose to approach a similar bit-rate.

The encoding time (including pre-encoding time for RDO-QPC) was collected to evaluate the algorithm complexity. A computer with the Microsoft Windows 7 system and the Intel Core i5-2400U CPU was used. The CPU frequency was 3.10 GHz. Compared with [6], the QPC technique in [10], RDO-QPC, and SRDO-QPC all achieve encoding time

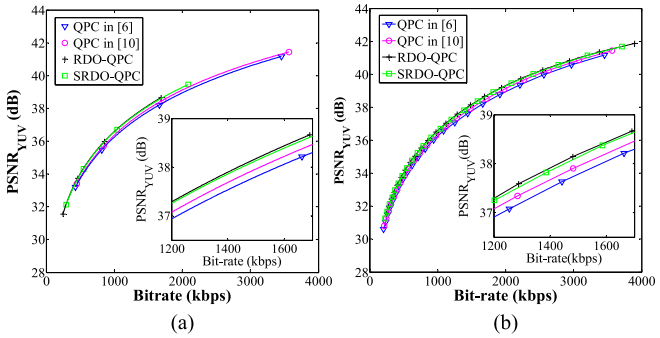

Fig. 10. R-D curves for *BasketballDrill*. (a) At the same QP_0 (22, 27, 32, 37). (b) At similar bit-rates.

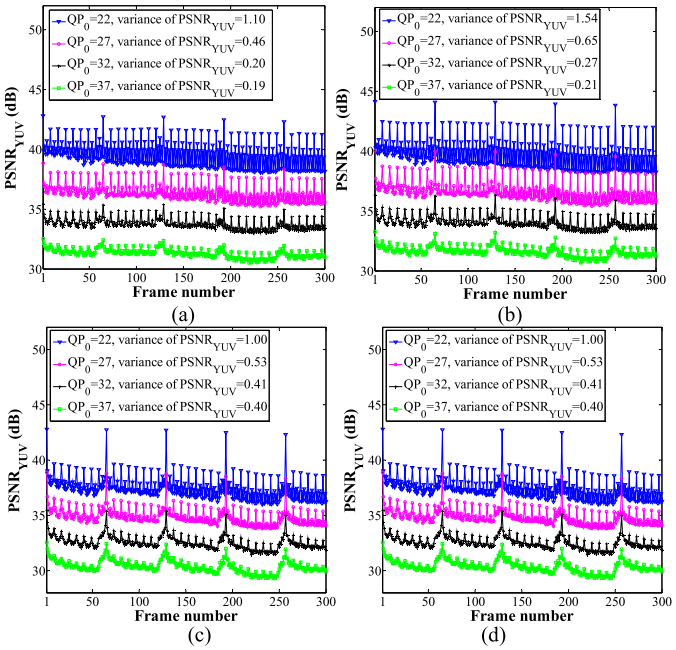

Fig. 11. $PSNR_{YUV}$ fluctuation for *BQSquare* sequence (GOP = 8). (a) [6]. (b) [10]. (c) RDO-QPC. (d) SRDO-QPC.

reduction by 0.57%, 7.73%, and 9.44%, respectively. The encoding times of RDO-QPC and SRDO-QPC are much less mostly because larger $x_l, l \geq 1$ are selected. It is seen that although RDO-QPC needs pre-encoding, both RDO-QPC and SRDO-QPC can be used in practical situations, meeting different requirements of computational complexity.

C. Quality Fluctuation

The issue of quality fluctuation over time is examined, where the average variance of $PSNR_{YUV}$ under the used QP_0 values is computed to evaluate the quality fluctuation degree for each video sequence. For all tested video sequences, the average variances of $PSNR_{YUV}$ are 1.25, 1.40, 1.49, and 1.46 for the QPC techniques in [6] and [10], RDO-QPC, and SRDO-QPC, respectively. Fig. 11 shows the $PSNR_{YUV}$ of each frame for *BQSquare* sequence encoded using the four QPC techniques with $QP_0 = 22$, 27, 32, and 37.

Generally speaking, larger $x_l, l \geq 1$ values lead to larger quality fluctuation. Therefore, the quality fluctuations resulted from the QPC technique in [10], RDO-QPC, and SRDO-QPC

TABLE IV
NUMBER OF SUBJECTS WHO PERCEIVED TPA

Sequence name	Number of subjects who perceived TPA (QP_0 = 22,27,32,37)			
	[6]	[10]	RDO-QPC	SRDO-QPC
Traffic	(0,0,0,0)	(0,0,0,0)	(0,0,0,0)	(0,0,0,0)
PeopleOnStreet	(0,0,0,0)	(0,0,0,0)	(0,0,0,0)	(0,0,0,0)
Nebuta	(0,0,0,0)	(0,0,0,0)	(0,0,0,0)	(0,0,0,0)
SteamLocomotive	(0,0,0,0)	(0,0,0,0)	(0,0,0,0)	(0,0,0,0)
Kimono	(0,0,0,0)	(0,0,0,4)	(0,0,0,0)	(0,0,0,5)
ParkScene	(0,0,0,0)	(0,0,0,2)	(0,0,0,0)	(0,0,0,2)
Cacuts	(0,0,0,0)	(0,0,0,0)	(0,0,0,3)	(0,0,0,0)
BasketballDrive	(0,0,0,0)	(0,0,0,0)	(0,0,0,0)	(0,0,0,0)
BQTerrace	(0,0,0,0)	(0,0,0,0)	(0,0,0,0)	(0,0,0,0)
BasketballDrill	(0,0,0,0)	(0,0,0,3)	(0,0,0,10)	(0,0,0,7)
BQMall	(0,0,0,0)	(0,0,0,6)	(0,0,5,29)	(0,0,5,29)
PartyScene	(0,0,0,0)	(0,0,0,0)	(0,0,0,25)	(0,0,0,6)
RaceHorses	(0,0,0,0)	(0,0,0,9)	(0,0,0,0)	(0,0,0,11)
BasketballPass	(0,0,0,6)	(0,0,2,10)	(0,0,9,24)	(0,0,9,24)
BQSquare	(0,0,3,17)	(0,0,9,26)	(0,0,13,24)	(0,0,13,24)
BlowingBubbles	(0,0,0,7)	(0,0,0,9)	(0,0,12,23)	(0,0,6,14)
RaceHorses	(0,0,0,6)	(0,0,0,7)	(0,0,6,16)	(0,0,10,21)
FourPeople	(0,0,0,3)	(0,0,0,2)	(0,0,0,17)	(0,0,0,12)
Johnny	(0,0,0,0)	(0,0,0,0)	(0,0,0,0)	(0,0,0,0)
KristenAndSara	(0,0,0,0)	(0,0,0,0)	(0,0,0,0)	(0,0,0,0)
Vidyo1	(0,0,0,6)	(0,0,3,11)	(0,0,2,23)	(0,0,3,16)
Vidyo3	(0,0,0,0)	(0,0,0,7)	(0,0,5,21)	(0,0,0,16)
Vidyo4	(0,0,0,0)	(0,0,0,0)	(0,0,0,12)	(0,0,0,7)
BasketballDrillText	(0,0,0,0)	(0,0,0,3)	(0,0,0,11)	(0,0,0,3)
ChinaSpeed	(0,0,0,0)	(0,0,0,3)	(0,0,0,0)	(0,0,0,2)
SlideEditing	(0,0,0,0)	(0,0,0,0)	(0,0,0,0)	(0,0,0,0)
SlideShow	(0,0,0,0)	(0,0,0,0)	(0,0,0,0)	(0,0,0,0)

are larger compared with that in [6]. However, it is noteworthy that quality fluctuation is not a problem if it is not perceivable to observers. So the following content is committed to subjective perception of the resulting quality fluctuation.

In [17], the perception of quality fluctuation in H.264/AVC/SVC with the hierarchical B structure has been studied. And we found that, at the low bit-rates, the quality fluctuation is easily perceived as an unwanted pumping artifact, i.e., the temporal pumping artifact (TPA), while the same degree of quality fluctuation may not be perceived at middle-to-high bit-rates.

In this paper, similar subjective experiments have been carried out to evaluate the perception of quality fluctuation using the four QPC techniques. Subjective experiments were carried out following the guidelines specified in [18], involving 30 nonexpert viewers who were not familiar with video processing. The reconstructed video sequences using different QPC techniques and QP_0 values were observed by viewers. The subjects were first given an example video with the TPA, and the standardized method of double stimulus impairment scale (DSIS) [18] was used for subjects to indicate whether they could perceive such an artifact when given different impaired sequences in the experiments. In the process of DSIS, each observer viewed an unimpaired reference video sequence followed by its impaired version. The videos were displayed at a viewing distance of four times height of pictures.

Table IV shows the number of subjects who perceived the TPA in the reconstructed video using different QP_0 and QPC techniques. According to Table IV, the following conclusions can be drawn. First, no quality fluctuation is perceived with

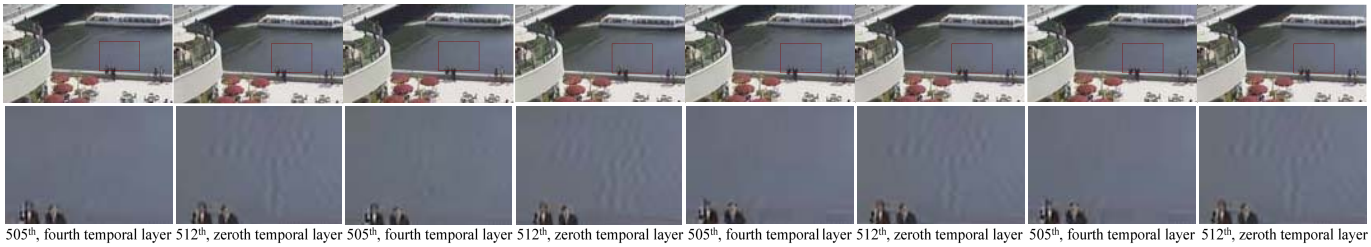

Fig. 12. 505th and 512th reconstructed frames of *BQSquare* sequence using different QPC techniques (GOP = 8). (a) [6] with $QP_0 = 37$. (b) [10] with $QP_0 = 37$. (c) RDO-QPC with $QP_0 = 37$. (d) SRDO-QPC with $QP_0 = 37$.

$QP_0 = 22$ and 27 in the tests using the four QPC techniques. And when $QP_0 = 32$, quality fluctuation is only perceived in 1, 3, 7, and 6 among the 27 tested video sequences using [6], [10], RDO-QPC, and SRDO-QPC, respectively. And it should be noted that in the above cases, the number of subjects who perceived quality fluctuation is less than half of the number of total subjects, and the perceived quality fluctuation, if there is any, was reported as very subtle. Therefore, generally speaking, at middle to high bit-rates (e.g., $QP_0 = 22$, 27, 32), quality fluctuation is hardly perceived using the proposed RDO-QPC, SRDO-QPC, [6], and [10]. Second, at low bit-rates (e.g., $QP_0 \geq 37$), however, quality fluctuation may be perceived in some video sequences as the TPA, and this problem exists for all compared QPC algorithms. In terms of TPA perception at low bit-rates (i.e., $QP_0 = 37$ in our test), the technique in [6] outperforms that in [10], RDO-QPC, and SRDO-QPC.

Therefore, it is safe to conclude that, at high or medium bit-rates, more quality fluctuation should be allowed, since it is hardly perceived by human eyes and this is beneficial for improving the R-D performance in video encoding. Actually, this is the spirit of the proposed RDO-QPC and SRDO-QPC. Furthermore, the subjective experiments show that the TPA sometimes appears at low bit-rates for H.265/HEVC using QPC techniques, while not for all cases. How to evaluate, quantify, reduce, or even eliminate the TPA at low bit-rates is an interesting and challenging topic. There are two other interesting issues regarding TPA perception. First, compared with H.264/AVC/SVC with the hierarchical B structure, the problem of TPA in H.265/HEVC using the random-access configuration is less serious. Second, TPA is less likely to be perceived in high-resolution video sequences compared with low-resolution video sequences.

Taking *BQSquare* for example, Fig. 12 intuitively shows the quality fluctuation issue, where the 505th and 512th reconstructed frames, which are located in the zeroth temporal layer and the highest temporal layer, respectively, are shown. In Fig. 12(a)–(d), the reconstructed frames are encoded using [6], [10], RDO-QPC, and SRDO-QPC, respectively, with $QP_0 = 37$. There are obvious texture variations of blur-clear in the region indicated by the red box as enlarged. In subjective experiments, most subjects perceived TPA in this region.

V. Conclusion

This paper proposes two R-D-optimization-based QPC techniques, i.e., RDO-QPC and SRDO-QPC, for the random-access configuration in H.265/HEVC. The experimental results verify that the proposed techniques can efficiently improve the R-D performance in video coding. For the video sequences with fast motion, the proposed RDO-QPC has a slight loss of R-D performance. It is noted that at low bit-rates, QPC techniques are likely to trigger the perception of TPA, which is an interesting and challenging issue to explore. The proposed RDO-QPC can also be incorporated into rate control for the random-access configuration in H.265/HEVC to achieve better R-D performance, which is currently under our investigation.

So far the issue of scene changes has not been considered in this paper. But, the proposed algorithm can be well adapted to the scenario with scene changes, where detection of scene changes is the key (while out of the scope of this paper). Once the scene change is detected, the first two frames can be pre-encoded to obtain the optimized QP for the subsequent frames in the same scene.

References

[1] H. Schwarz, D. Marpe, and T. Wiegand, "Overview of the scalable video coding extension of the H.264/AVC standard," *IEEE Trans. Circuits Syst. Video Technol.*, vol. 17, no. 9, pp. 1103–1120, Sep. 2007.

[2] H. Schwarz, D. Marpe, and T. Wiegand, "Analysis of hierarchical B pictures and MCTF," in *Proc. IEEE Int. Conf. Multimedia Expo.*, Toronto, ON, Canada, Jul. 2006, pp. 1929–1932.

[3] H. Schwarz, D. Marpe, and T. Wiegand, *Hierarchical B Pictures*, document JVT-P014, Joint Video Team, Poznań, Poland, Jul. 2005.

[4] *Information Technology—High Efficiency Coding and Media Delivery in Heterogeneous Environments—Part 2: High Efficiency Video Coding*, document Rec. H265 and ISO/IEC 23008-2:2013, Apr./Nov. 2013.

[5] G. J. Sullivan, J.-R. Ohm, W.-J. Han, and T. Wiegand, "Overview of the High Efficiency Video Coding (HEVC) standard," *IEEE Trans. Circuits Syst. Video Technol.*, vol. 22, no. 12, pp. 1649–1668, Dec. 2012.

[6] K. McCann, C. Rosewarne, B. Bross, M. Naccari, K. Sharman, and G. Sullivan, *High Efficiency Video Coding (HEVC) Test Model 16 (HM16) Improved Encoder Description*, document JCTVC-S1002, Jonit Collaborative Team on Video Coding, Strasbourg, France, Oct. 2014.

[7] X. Li, P. Amon, A. Hutter, and A. Kaup, "Adaptive quantization parameter cascading for hierarchical video coding," in *Proc. IEEE Int. Symp. Circuits Syst.*, Paris, France, May/Jun. 2010, pp. 4197–4200.

[8] X. Li, X. Guo, and S. Lei, *CE4 Subtest 2: Adaptive De-Quantization Offset*, document JCTVC-G278, Geneva, Switzerland, Nov. 2011.

[9] X. Yu, J. Wang, D. He, and G. Martin-Cocher, *CE4 Subtest 2.2: Quantization With Adaptive Reconstruction Levels*, document JCTVC-G382, Geneva, Switzerland, Nov. 2011.

[10] B. Li, D. Zhang, H. Q. Li, and J. Z. Xu, *QP Determination by Lambda Value*, document JCTVC-I0426, Joint Collaborative Team on Video Coding, Geneva, Switzerland, May 2012.

[11] F. Bossen, *Common HM Test Conditions and Software Reference Configurations*, document JCTVC-L1100, Feb. 2013.

[12] *High Efficiency Video Coding (HEVC) Test Model 14 (HM 14) Encoder*, accessed on Apr. 2014. [Online]. Available: https://hevc.hhi.fraunhofer.de/svn/svn_HEVCSoftware/branches/
[13] B. Li, H. Q. Li, L. Li, and J. L. Zhang, *Rate Control by R-Lambda Model for HEVC*, document JCTVC-K0103, Joint Collaborative Team on Video Coding, Shanghai, China, Oct. 2012.
[14] S. Pateux and J. Jung, *An Excel Add-In for Computing Bjontegaard Metric and Its Evolution*, document VCEG-AE07, Marrakesh, Morocco, Jan. 2007.
[15] A. Ben-Israel, "A Newton–Raphson method for the solution of systems of equations," *J. Math. Anal. Appl.*, vol. 15, no. 2, pp. 243–252, Aug. 1966.
[16] J. R. Ohm, G. J. Sullivan, H. Schwarz, T. K. Tan, and T. Wiegand, "Comparison of the coding efficiency of video coding standards—Including High Efficiency Video Coding (HEVC)," *IEEE Trans. Circuits Syst. Video Technol.*, vol. 22, no. 12, pp. 1669–1684, Dec. 2012.
[17] S. Wan, Y. Gong, and F. Yang, "Perception of temporal pumping artifact in video coding with the hierarchical prediction structure," in *Proc. IEEE Int. Conf. Multimedia Expo.*, Melbourne, VIC, Australia, Jul. 2012, pp. 503–508.
[18] *Methodology for the Subjective Assessment of the Quality of Television Pictures*, document ITU-R Rec. ITU-RBT. 500-13, Jan. 2012.

Yanchao Gong received the B.E. degree in electronic information engineering from Shandong University of Technology in 2010 and the M.E. degree in signal and information processing from Northwestern Polytechnical University, Xi'an, China, in 2013, where he is currently working toward the Ph.D. degree in the School of Electronics and Information.

His research interests include video coding optimization, and video quality assessment.

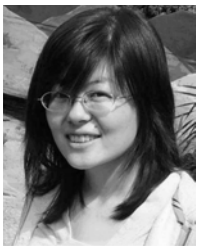

Shuai Wan (S'06–M'08) received the B.E. degree in telecommunication engineering and M.E. degree in communication and information system from Xidian University, Xi'an, China, in 2001 and 2004, respectively, and the Ph.D. degree in electronic engineering from Queen Mary, University of London in 2007.

She is now a Professor in Northwestern Polytechnical University, Xi'an, China. Her research interests include scalable/multiview video coding, video quality assessment, and hyperspectral image compression.

Kaifang Yang received the B.E. degree in telecommunication engineering from Xi'an Technological University in 2010 and the M.E. degree in signal and information processing from Northwestern Polytechnical University, Xi'an, China, in 2013, where she is currently working toward the Ph.D. degree.

Her research interests include video coding optimization, and video quality assessment.

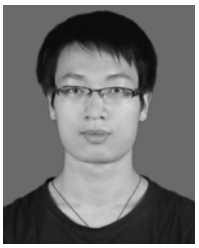

Yuan Yang received the B.E. degree in communications engineering from Northwestern Polytechnical University, Xi'an, China, where he is currently working toward the M.S. degree.

His research interest is video coding optimization.

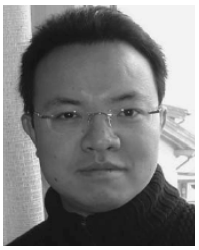

Bo Li received the B.E., M.S., and Ph.D. degrees in communications engineering from Xidian University, Xi'an, China, in 1994, 1996, and 2002, respectively.

From 2002 to 2004, he was a Postdoctoral Researcher with the University of Trento, Trento, Italy. He is currently a Full-Time Professor with the School of Electronics and Information, Northwestern Polytechnical University, Xi'an, China. His current research interests include multimedia wireless communication networks, cross-layer design of wireless communications systems, and resource allocations.